Research Repository UCD

Title	Particle Migration and Clogging in Porous Media: A Convergent Flow Microfluidics Study
Authors(s)	Liu, Q, Zhao, Budi, Santamarina, J. Carlos
Publication date	2019-09
Publication information	Liu, Q, Budi Zhao, and J. Carlos Santamarina. "Particle Migration and Clogging in Porous Media: A Convergent Flow Microfluidics Study." Wiley, September 2019. https://doi.org/10.1029/2019JB017813.
Publisher	Wiley
Item record/more information	http://hdl.handle.net/10197/12590
Publisher's version (DOI)	10.1029/2019JB017813

Downloaded 2026-05-01 23:34:05

The UCD community has made this article openly available. Please share how this access benefits you. Your story matters! (@ucd_oa)

© Some rights reserved. For more information

Particle Migration and Clogging in Porous Media: A Convergent-Flow Microfluidics Study

Q. Liu[1], B. Zhao[1], J. C. Santamarina[1]

Abstract

The migration and retention of fine particles in porous media are important phenomena in natural processes and engineering applications. Migrating particles experience physicochemical interactions with carrier fluids, pore walls and other migrating particles. The governing dimensionless ratios capture particle-level forces, flow conditions, and geometric characteristics. This study explores micron-size particle migration and retention in microfluidic chips during convergent radial flow, which is the prevalent flow condition in water extraction and oil production. Pore-scale observations reveal the role of electrostatic interactions on clogging mechanisms: glass particles experience retardation-accumulation-bridging, while quasi-buoyant latex particles involve capture-&-clogging. Consequently, flow rates exert opposite effects on the clogging behavior of inertial glass particles versus electrostatically-affected latex particles. Migrating particles experience a varying fluid velocity field in convergent radial flow and clogging reflects the evolving local conditions (N_{ad}, Ar, Stk, and Re). In particular, clogged pores alter local flow and promote further clogging nearby. Pore network model simulations suggest that such "dependent clogging" lowers the permeability of the porous medium more effectively than independent clogging at random locations.

Keywords: Particle migration, porous media, radial flow, interception, retardation, clogging

Corresponding author: B. Zhao (budi.zhao@kaust.edu.sa)

Affiliation: [1]Earth Science and Engineering, King Abdullah University of Science and Technology (KAUST), Thuwal 23955-6900, Saudi Arabia.

List of Notations

d	Migrating particle diameter
d_c	Constriction size
D	Obstacle size
Gs	Specific gravity
ρ_p	Particle mass density
ρ_f	Fluid mass density
μ	Fluid viscosity
v	Fluid velocity
G	Gravity
N_{ad}	Adhesion number
Ar	Archimedes number
Stk	Stokes number
N_G	Geometric ratio
Re	Reynolds number
V	Permeated volume
q	Flow rate
η_{DI}	Capture efficiency
P_{dep}	Probability of dependent clogging
P_{ind}	Probability of independent clogging

INTRODUCTION

The migration and retention of fine particles in porous media are critically important to natural processes and engineering applications such as soil erosion (Aitchison and Wood, 1965; Jones, 1971), groundwater flow (Ryan and Elimelech, 1996), oil production (Khilar and Fogler, 1983; Mungan, 1965) and the performance of geothermal reservoirs (You *et al.*, 2015). Clogging at pore throats reduces the permeability of the medium and changes flow patterns (Muecke, 1979; Krueger, 1988).

Migrating particles experience physicochemical interactions with carrier fluids, pore walls and other migrating particles (McDowell et al. 1986). The resulting particle-level forces include the buoyant weight, inertia, drag, and particle-wall interaction forces. Interaction forces and the constriction-to-particle size ratio d_c/d play a central role in clogging (Sakthivadivel and Einstein 1970; Sherard et al. 1984; Valdes and Santamarina 2008; Marin et al. 2018). In the extreme case of $d_c/d \rightarrow 1.0$, large particles or large particle aggregations cause clogging by sieving (Sauret *et al.*, 2014; Dersoir *et al.*, 2015; Dersoir *et al*., 2017). In addition, the probability of clogging depends on the volume fraction of migrating particles (Valdes and Santamarina, 2006; Wyss *et al.*, 2006), path tortuosity (Kampel et al. 2009; Bacchin et al. 2014), and ensuing inertial retardation (Valdes and Santamarina 2007).

Convergent radial flow is the prevailing flow condition in water extraction and oil production operations. Drag and inertial particle-level forces evolve from the far field to the wellbore because of the spatially varying fluid velocity field. Yet, limited research to date has been reported on the influence of radial flow on clogging patterns and changes in permeability. Furthermore, there is also limited insight about the migration and retention of fine-grained particles

affected by electrical interactions, i.e. micro and submicron size particles (Valdya and Fogler, 1992; Liu *et al.*, 2019).

Microfluidic devices allow the direct observation of migrating fines and pore clogging in porous media (see Dressaire and Sauret 2017 for a detailed review). This study explores micron-scale particle migration and retention during convergent radial flow within microfluidic chips and places emphasis on electrostaic interactions, inertial and drag forces, geometric ratios and causal links between clogging events.

EXPERIMENTAL STUDY: MATERIALS AND METHODS

Microfluidic Chips

We use soft lithography to fabricate microfluidic chips for convergent radial flow. The process includes: (i) mask layout using computer-aided design software, (ii) mask printing, (iii) fabrication of the silicon wafer master with negative photoresist (SU-8 2050), (iv) polymerization of polydimethylsiloxane PDMS using the master as a mold, and (v) bonding of the PDMS slabs onto a glass substrate with the use of oxygen plasma (see Mazutis et al. 2013 for a detailed protocol). The microfluidic chip consists of 300 μm cylindrical columns separated by d_c=40 μm wide pore constrictions; all pore channels are 50 μm high. The inlet cavity ahead of the porous-network ensures a uniform flow field (Figure 1-a).

Particle Suspensions

We use glass particles (440345 and 44054, Sigma-Aldrich, specific gravity Gs=2.60) and polystyrene latex particles (polystyrene plain, PS010UM and PS005UM, Magsphere, Gs=1.05) of two diameters d= 5 μm and 10 μm. These four particle types create different conditions among

70 governing forces and geometric ratios (constriction-to-particle size ratios d_c/d=4 and 8, Figure 1-
71 b). All particle suspensions are prepared with deionized water at a 0.2% mass concentration.

72 ***Test Protocol***

73 Figure 1-c presents the flow system. We saturate the radial flow microfluidic chip with deionized
74 water (trapped air escapes through the gas-permeable PDMS walls), and use a peristaltic pump to
75 withdraw the suspensions from the "central port" at a constant flow rate (PeriWave microfluidic
76 pump). A pressure sensor monitors the pressure at the central port (uPS0250, LabSmith). A
77 magnetic stirrer prevents settlement or coagulation prior to injection. Digital video microscopy
78 records particle movements within pores and captures emerging clogging patterns at the chip-scale.

79 ***Image Analysis***

80 We wrote an image processing algorithm to automatically detect pore clogging events at any of
81 the 1078 constrictions parallel to the flow direction in the full chip. The algorithm extracts the
82 image of each constriction and assesses clogging based on (1) the grey value relative to the
83 maximum, minimum and threshold grey values, and (2) the total number of pixels in the dark area
84 (red box, Figure 2). Data gathered with the calibrated algorithm allow the interpretation of spatial
85 and temporal correlation among clogging events.

86 **RESULTS AND ANALYSES**

87 ***Dimensionless Ratios***

88 A migrating particle experiences its buoyant weight, the drag force, inertia against motion changes,
89 and electrical attraction towards other particles and the pore walls. Dimensionless ratios capture

the governing processes in terms of the particle size d, obstacle size D, particle mass density ρ_p, fluid mass density ρ_f, fluid viscosity μ, fluid velocity v, gravity g, and attraction force F_A to pore walls (the sum of van der Waals force, electrostatic force and hydrophobic adhesion force). The three main dimensionless ratios are:

Adhesion number: $$\mathrm{N_{ad}} = \frac{\text{Attraction}}{\text{Drag}} = \frac{F_A}{3\pi\mu d v} \quad (1)$$

Archimedes number: $$\mathrm{Ar} = \frac{\text{Terminal velocity}}{\text{Flow velocity}} = \frac{g d^2 (\rho_p - \rho_f)}{\mu v} \quad (2)$$

Stokes number: $$\mathrm{Stk} = \frac{\rho_p d^2 v}{18 \mu D} \quad \text{(Inertial effect)} \quad (3)$$

The Stokes number Stk is the ratio between the particle response time to the fluid field response time; a particle with a large Stokes number is dominated by inertia and tends to follow its trajectory, while a particle with a low Stokes number follows fluid streamlines. The ratio N_G between the constriction size d_c and the size of the migrating particle d is the main geometric descriptor:

Geometric ratio: $$N_G = d_c/d \quad (4)$$

In addition, the Reynolds number $\mathrm{Re} = \rho_f v D/\mu$ characterizes flow conditions around an obstacle.

Clogging Mechanisms

Figure 3 illustrates salient pore-scale observations gathered for the four particle suspensions. Distinct clogging mechanisms take place when *glass particles* and *latex particles* are involved.

Glass particles. Non-buoyant glass particles (specific gravity Gs=2.60) experience gravity and fall towards the bottom substrate (high Ar value); on the other hand, their inertia causes collisions against obstructing pore walls (high Stk, Figure 4-a), and particles suffer significant retardation relative to the fluid displacement along the flow paths. Inertial retardation develops where streamlines bend and the flow velocity changes at a high Stokes number Stk. Retardation results in a gradual increase in the local volume fraction of particles at the pore scale (Figure 3). High local concentrations near pore constrictions facilitate the formation of granular bridges. Figure 4-b illustrates the retardation-accumulation-bridging process.

Dimensionless ratios Ar and Stk scale with the square of the particle size d^2, hence, retardation becomes negligible when particles are small. Figure 3 shows no evidence of retardation and accumulation for the d=5 μm glass particle suspension.

Clogging for a geometric ratio N_G=4 (Figure 3- top left) exceeds previously reported thresholds from single pore constriction experiments with spherical particles that showed stable bridge formation when N_G<3 (Marin et al. 2018; Valdes and Santamarina 2006). This result hints to stabilizing electrostatic effects when small micron-scale particles are involved. Furthermore, a clogged pore throat in porous medium alters flow pathways instead of generating a large pressure drop across the clogged pore throat, which is the case for the single channel systems. Both effects combine to allow for bridging at N_G values larger than 3 when small particles migrate in pore networks.

Latex particles. Quasi-buoyant latex particles (Gs=1.05) experience negligible retardation and follow along streamlines (Ar≈ 0 and small Stk). However, latex particles experience attraction towards PDMS walls and may be captured if in close proximity (high adhesion number N_{ad}).

Figure 4-c illustrates the process of direct particle interception. Indeed, latex particles experience a high adhesion number N_{ad} towards the hydrophobic PDMS pore walls which ensures a strong particle-surface bonding. Captured particles reduce the size of pore throats, and particle-particle interaction favors aggregate formation near constrictions (Dersoir *et al.*, 2015; Dersoir *et al*., 2017). Reduced constriction size and grain aggregation combine to form bridges even at large constriction-particle size ratios N_G (N_G=4 and 8 - Figures 3 and 4). The sequence of time-lapse photographs shown in Figure 5 highlights the capture-clogging process at pore constrictions.

The Effect of Flow Rate

Experimental results suggest that both particle retardation and capture are flow velocity dependent (Note: velocity *v* is involved in governing dimensionless ratios N_{ad}, Ar, Stk and Re). We study the influence of the suspension injection rate on clogging at the pore scale using the convergent radial flow chips (Figure 1). The Reynolds number is Re<35 in all experiments. Let's define the clogging ratio as the number of clogged pore constrictions with respect to the total number of constrictions. Figure 6 shows the effect of flow rate on the clogging ratio evolution for both glass and latex particles.

Clearly, a high flow rate leads to fewer clogged pores for glass particles (Figure 6-a). The prevalent retention mechanism for glass particles is retardation-accumulation-bridging. A high flow rate decreases the Archimedes number Ar and minimizes gravity retardation (the maximum Archimedes number for the various flow rate is: Ar_{max}=2 when *q*=20 μL/min, Ar_{max}=1 when *q*=40 μL/min, and Ar_{max}=0.7 when *q*=20 μL/min).

The flow rate exerts a reversed effect on the clogging behavior of latex particles compared to glass particles (Figure 4-b): the clogging ratio increases with the increase in flow rate q from q=20 μL/min (Re_{max}=11) to q=60 μL/min (Re_{max}=33). Streamlines compress at high Reynolds numbers and improve particle "capture efficiency by direct interception" η_{DI} (Figure 4-c). A detailed hydrodynamic formulation by Espinosa-Gayosso et al. (2012) shows the relationship between the capture efficiency η_{DI}, Reynolds number Re and the relative size d/D between the migrating particle size d and the obstacle size D. Their results can be approximated as (valid for passive particles and Re≤47):

$$\log \eta_{DI} = 0.4 \log Re + 6(d/D) - 3 \quad (5)$$

Hence, the particle capture efficiency by direct interception η_{DI} increases with both Reynolds number Re and the particle-to-obstacle size ratio d/D.

The Effect of Radial Flow

The spatially varying velocity field in convergent radial flow changes local dimensionless ratios Ar, Stk, N_{ad}, Re from the far-field to the central producing well. Figure 7 shows the evolution of row clogging ratios in the radial-flow microfluidic chip during the injection of 500 pore volumes at two different flow rates. The clogging ratio for glass particles decreases linearly from the far-field to the central port as glass particles experience higher gravity retardation far from the central extraction port (Figure 7-a+b).

On the other hand, streamline compression at high flow velocity increases the capture efficiency of latex particles (Figure 4-c, Equation 5); yet, the very high near-well velocity drags particles away and hinders capture (low N_{ad}). These two competing mechanisms lead to a

maximum clogging ratio at a characteristic radial distance away from the well wall (Note: annular clogging was reported in Valdes and Santamarina, 2006).

Dependent Clogging - Implications

Experimental observations show that a clogged pore constriction alters the flow patterns in nearby open paths, affects retardation, and may promote further clogging. We wrote a post-processing algorithm to quantify the spatial dependence of clogging in convergent radial flow. Let's call a new clogging event "*dependent"* when one or more of the neighboring pore constrictions are already clogged; otherwise the new clogging event is called "*independent"* (Figure 8-a). Figure 8-b and c show the evolving clogging ratios for dependent and independent pore clogging events in the case of glass and latex particles under the same flow rate q=40 μL/min. The increment of the clogging ratio $\Delta N/N_{ava}$ is calculated within 5-minute time intervals, given the fact that the number of open pore constrictions for dependent/ independent clogging N_{ava} evolves with time. Dependent clogging is significantly more frequent than independent clogging, especially for glass particles due to the heightened inertial retardation in the surroundings. These results underscore the "cross-talk" between pores observed in parallel microchannel experiments (Liot *et al.*, 2018; Sauret *et al.*, 2018; Van Zwieten *et al.*, 2018).

The distribution of clogged pore throats profoundly influences the reduction in permeability of porous media (Dai and Seol, 2014; Sauret *et al.*, 2018). We use a simple pore network model to explore the effect of dependent clogging on the evolution of permeability. The porous medium is a 2-D square network model made of 50×50 tubes of the same radius. Each clogging event is treated as a random event. Initially, all constrictions have the same clogging probability P_{ind}. We assume Hagen-Poiseuille flow in each tube until it clogs; thereafter the

conductivity of the tube becomes zero. Once a tube clogs, neighboring tubes have a dependent probability of clogging P_{dep}. Figure 9 shows the influence of P_{dep}/P_{ind} on the evolution of permeability. Clearly, spatially correlated dependent clogging lowers the permeability of the porous medium more effectively than independent clogging.

CONCLUSIONS

Migratory particles in porous media interact with fluids, pore walls, and other particles. Dimensionless ratios capture the effect of particle-level forces (N_{ad}, Ar, and Stk), flow conditions (Re), and geometric characteristics (N_G). These ratios define the domains for particle retardation, adhesion, and bridging.

Micron-scale non-buoyant glass particles and quasi-buoyant latex particles exhibit distinct clogging mechanisms. Glass particles experience retardation from gravity and inertial effects; the increase in the local volume fraction of particles promotes the formation of multi-grain bridges at pore constrictions. Quasi-buoyant latex particles emphasize electrical interactions and may adhere to pore walls. Captured latex particles and aggregates may eventually plug constrictions, even at relatively high geometric ratios N_G.

Flow rates exert opposite effects on the clogging behavior of glass and latex particles. A high flow rate diminishes gravity retardation and hinders the formation of stable multi-grain bridges (case: non-buoyant glass particles). On the other hand, high flow rates compress streamlines and facilitate adhesive capture to pore walls (case: quasi-buoyant latex particles).

Particles experience varying fluid velocity fields in convergent radial flow. Therefore, clogging distributions in radial-flow reflect the local conditions (N_{ad}, Ar, Stk, and Re). Glass

213 particles show a higher clogging ratio in the far-field (gravity retardation under low flow velocity),
214 while electrically affected latex particles tend to clog pores at a characteristic distance from the
215 well wall and form an annular clogging pattern.

216 Clogging in porous media is not a random process. In particular, clogged pores alter flow
217 conditions and promote further clogging nearby. Pore network model simulations suggest that
218 dependent clogging lowers the permeability of the porous medium more effectively than
219 independent clogging.

220

221 **ACKNOWLEDGEMENTS**

222 Support for this research was provided by the KAUST endowment. G. E. Abelskamp edited the
223 manuscript. Datasets presented as part of this study are available from the KAUST Repository
224 (http://hdl.handle.net/10754/656179).

225

226

227

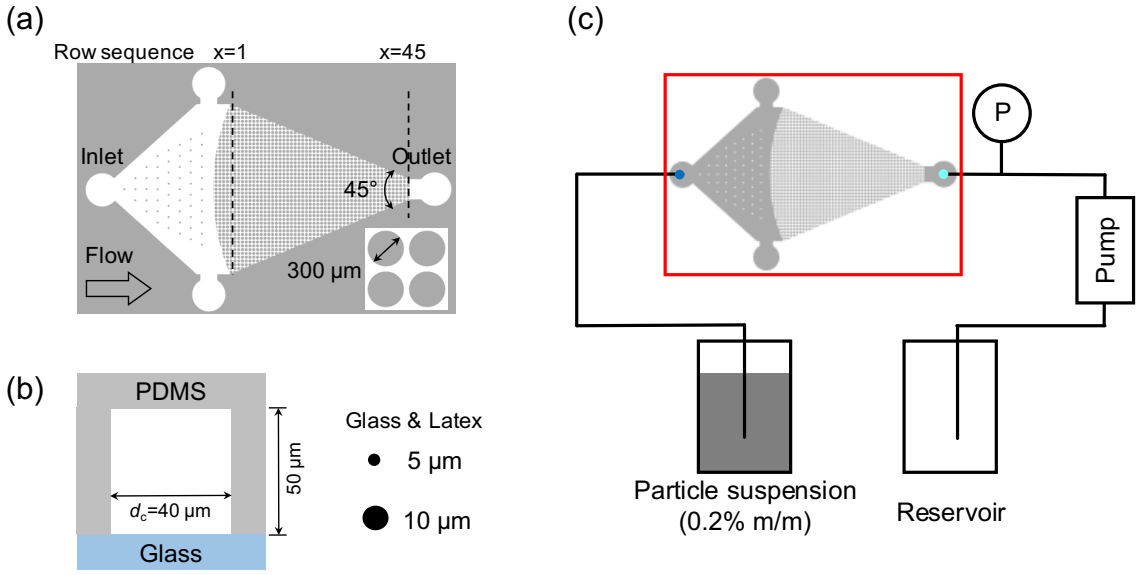

228

229 Figure 1. Microfluidics system. (a) Radial flow chip. (b) Cross section of a pore constriction and the relative
230 sizes of particles used in this study. (c) Flow system (P: pressure transducer).

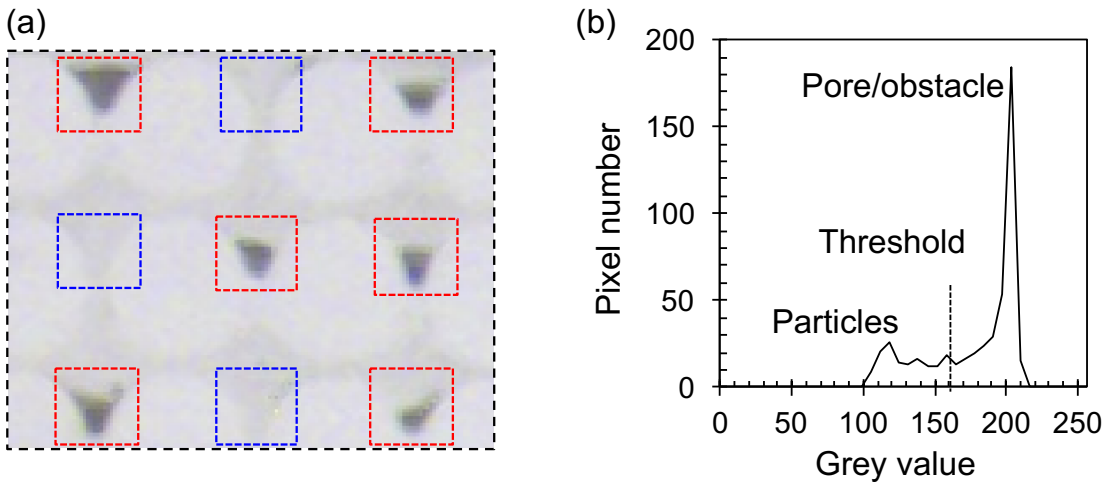

Figure 2. Image analysis. (a) The plugged constrictions shown within red boxes are identified by the image analysis algorithm. (b) Grey value distribution of a pore constriction.

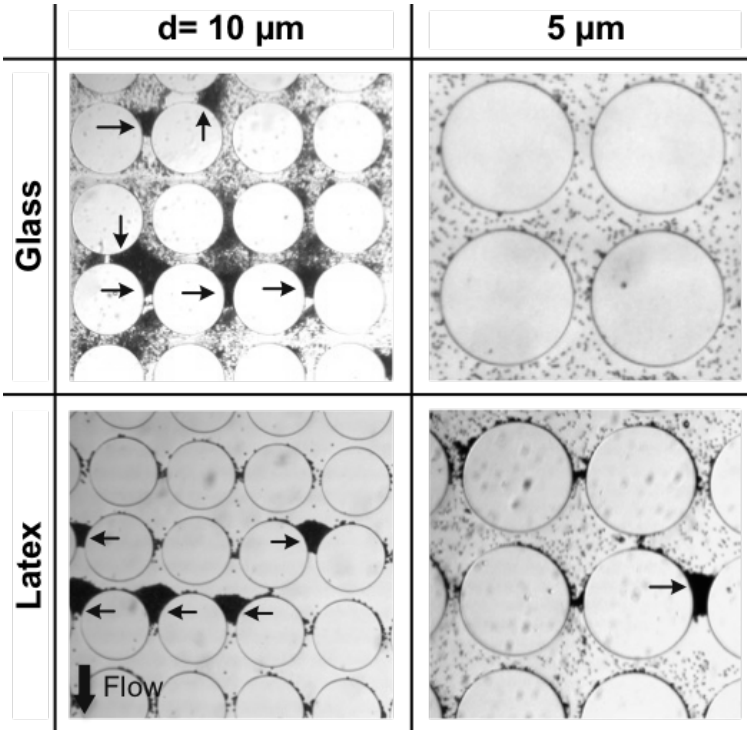

Figure 3. Clogging: pore-scale observations. The solid columns are 300 µm in diameter in all cases (refer to Figure 1). Note: there is no clogging with 5 µm glass particles.

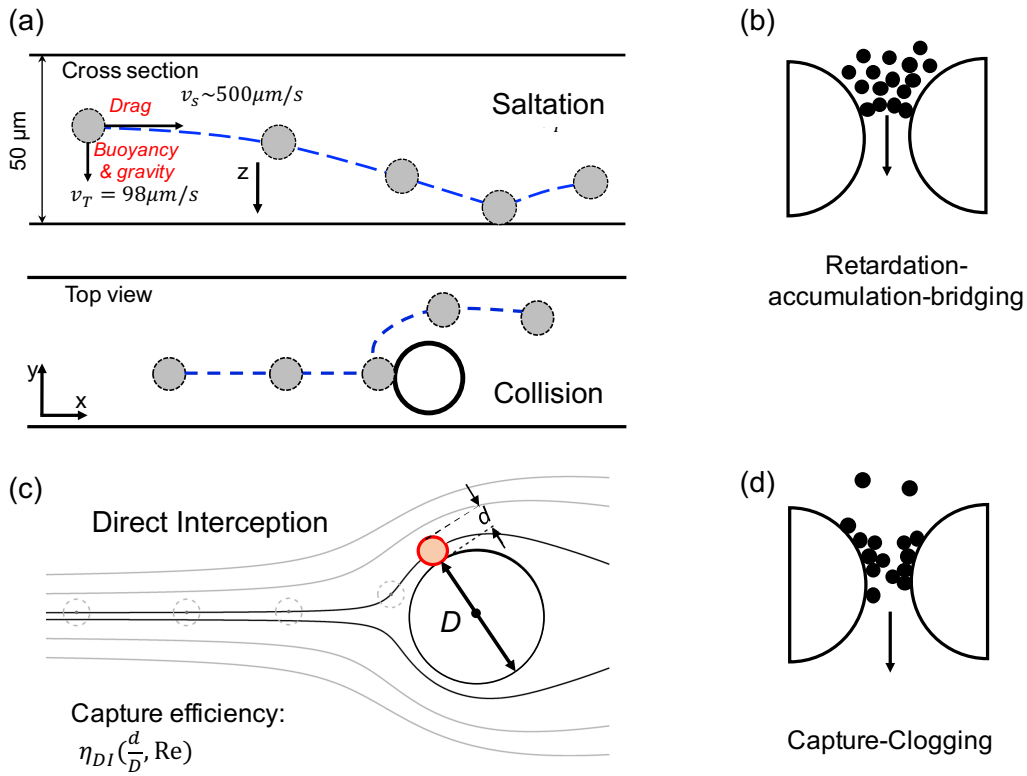

240

241 Figure 4. Clogging mechanisms. (a) Gravity retardation and inertial retardation. (b) Sketch of the
242 retardation-accumulation-bridging process. (c) Direct interception (modified from Espinosa- Gayosso et
243 al. 2012). (d) Sketch of the capture-clogging process.

244

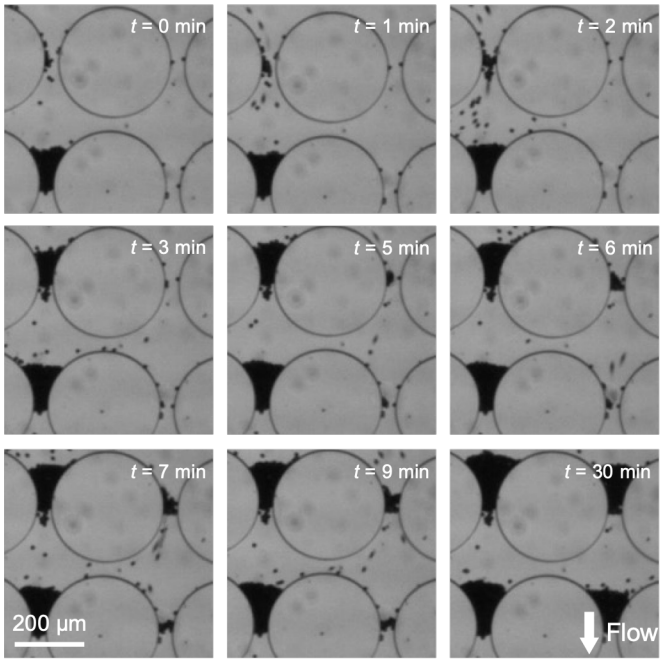

Figure 5. Time lapse photographs: clogging sequence for migrating 10 µm latex particles ($N_G=d_c/d=4$).

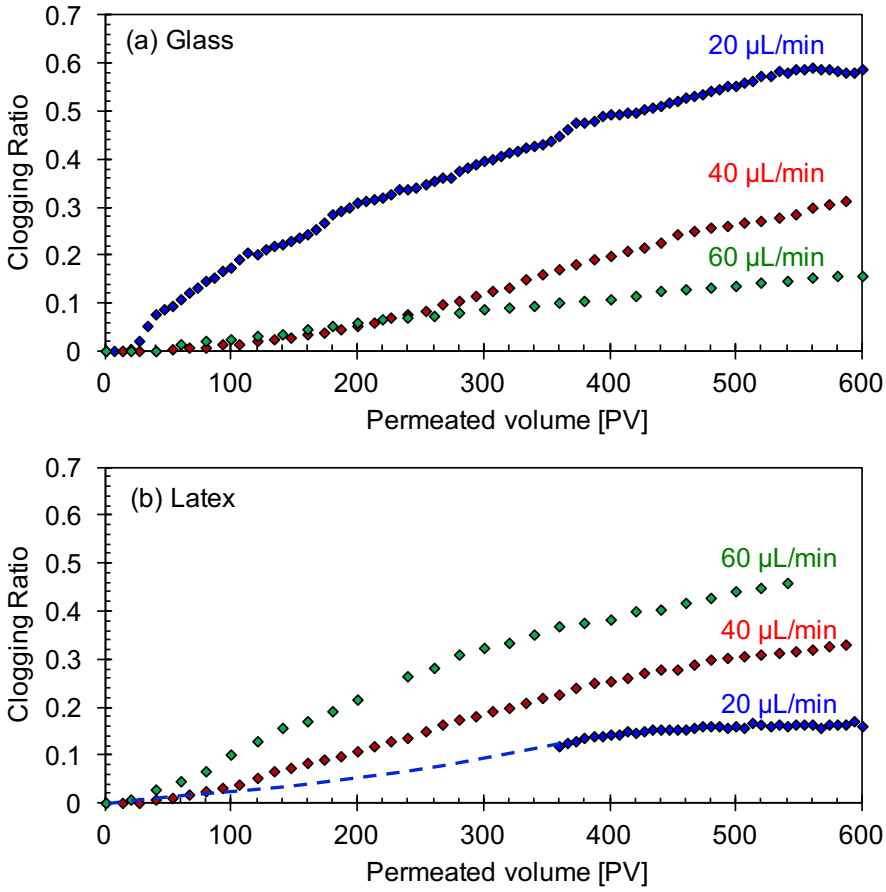

247

248 Figure 6. The effect of flow rate on the evolution of clogging. (a) Glass particles. (b) Quasi-buoyant latex
249 particles. Flow rates q= 20µL/min, 40µL/min, and 60µL/min. In both cases: d=10 µm.

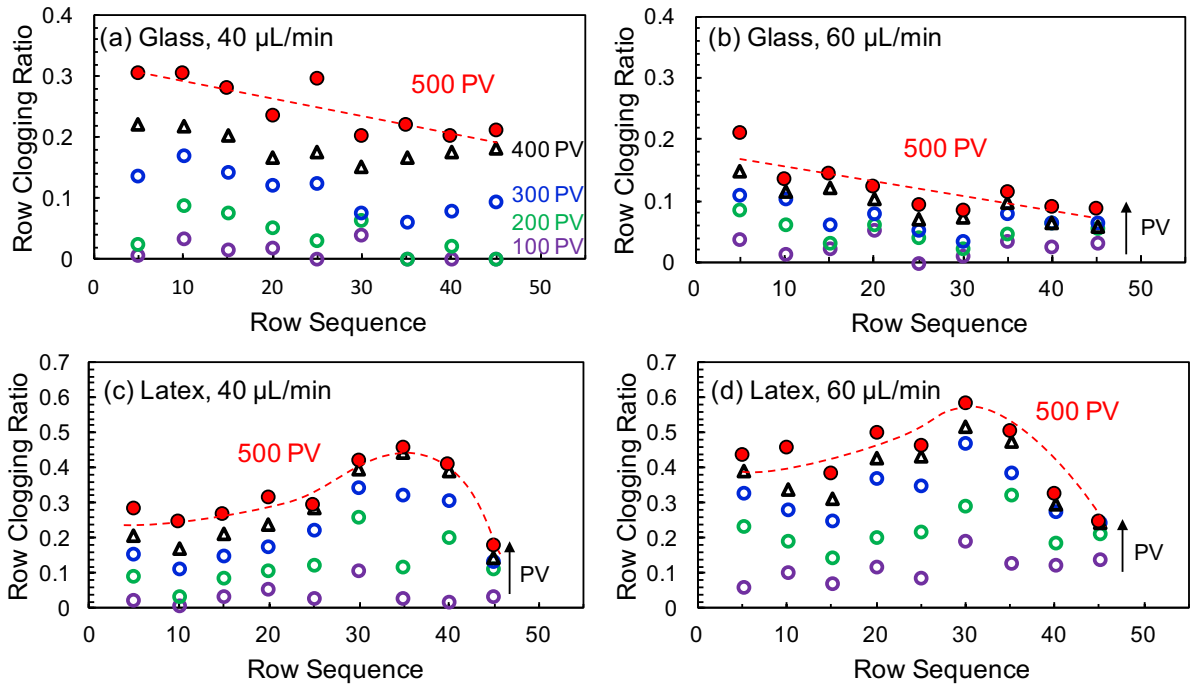

250

251 Figure 7. Evolution of clogging ratio distribution across radial-flow microfluidic chips from 0 to 500
252 permeated pore volumes. Glass particles: (a) flow rate q=40 µL/min, and (b) q=60 µL/min. Latex particles:
253 (c) flow rate q=40 µL/min, and (d) q=60 µL/min. The row sequence is defined in Figure 1-a. In all cases,
254 d=10 µm, so that $N_G=d_c/d=4$. Refer to (a) for color coding of pore volumes.

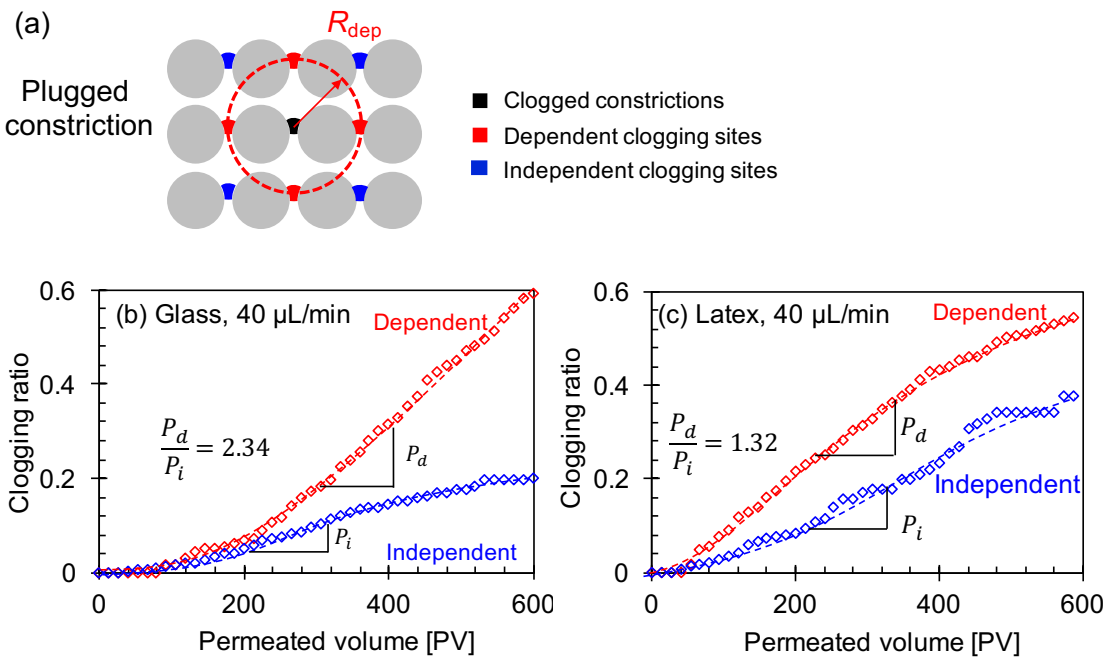

255

256 Figure 8. Dependent vs. independent clogging. (a) Definition of dependent clogging. Cumulative dependent
257 and independent clogging ratios: (b) glass particles and (c) latex particles. Flow rate q=40 μL/min. The
258 clogging ratio is $\sum \Delta N / N_{ava}$ where ΔN is the incremental number of clogged pore constrictions and N_{ava} is
259 the number of open pore constrictions.

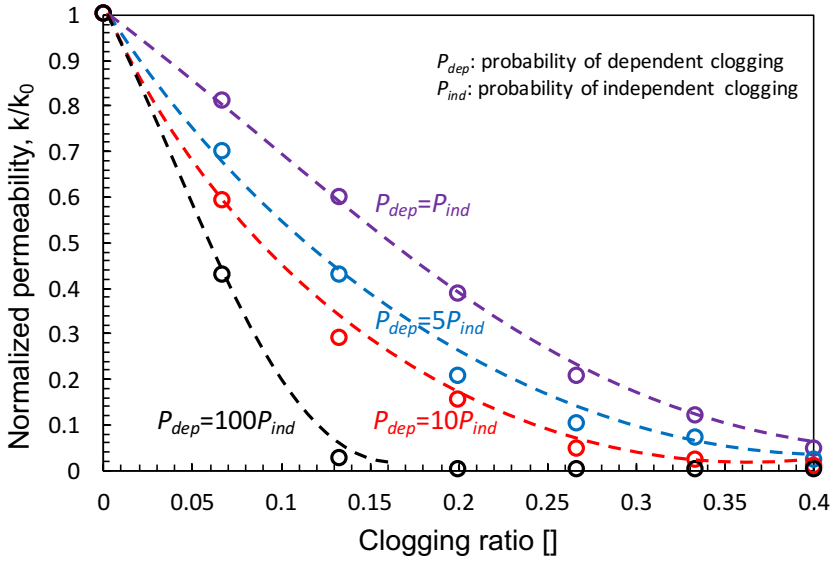

Figure 9. The effect of dependent clogging on permeability reduction – Pore network model simulations. The vertical axis shows the evolution of permeability k normalized by the permeability of the unclogged medium k_0.

REFERENCE

Aitchison, G. D., & Wood, C. C. (1965). Some interactions of compaction, permeability and post-construct ion deflocculation affecting the probability of piping failure in small earth dams. Proceeding of the 6th international conference on soil mechanics and foundation engineering, 442 - 446.

Bacchin, P., Derekx, Q., Veyret, D., Glucina, K., & Moulin, P. (2014). Clogging of microporous channels networks: Role of connectivity and tortuosity. Microfluidics and Nanofluidics, 17(1), 85–96. https://doi.org/10.1007/s10404-013-1288-4

Dai, S., & Seol, Y. (2014). Water permeability in hydrate ‐ bearing sediments: A pore ‐ scale study. Geophysical Research Letters, 41(12), 4176 ‐ 4184. https://doi.org/10.1002/2014GL060535

Dersoir, B., Schofield, A. B., & Tabuteau, H. (2017). Clogging transition induced by self filtration in a slit pore. Soft Matter, 13(10), 2054–2066. https://doi.org/10.1039/c6sm02605b

Dersoir, Benjamin, de Saint Vincent, M. R., Abkarian, M., & Tabuteau, H. (2015). Clogging of a single pore by colloidal particles. Microfluidics and Nanofluidics, 19(4), 953–961. https://doi.org/10.1007/s10404-015-1624-y

Dressaire, E., & Sauret, A. (2017). Clogging of microfluidic systems. Soft Matter, 13(1), 37–48. https://doi.org/10.1039/C6SM01879C

Espinosa-Gayosso, A., Ghisalberti, M., Ivey, G. N., & Jones, N. L. (2012). Particle capture and low-Reynolds-number flow around a circular cylinder. Journal of Fluid Mechanics, 710, 362–378. https://doi.org/10.1017/jfm.2012.367

Jones, A. (1971). Soil Piping and Stream Channel Initiation. Water Resources Research, 7(3), 602–610. https://doi.org/10.1029/WR007i003p00602

Kampel, G., Goldsztein, G. H., & Santamarina, J. C. (2009). Particle transport in porous media: The role of inertial effects and path tortuosity in the velocity of the particles. Applied Physics Letters, 95(19), 1–4. https://doi.org/10.1063/1.3263718

Khilar, K. C., & Fogler, H. S. (1983). Water Sensitivity of Sandstones. Society of Petroleum Engineers Journal, 23(01), 55–64. https://doi.org/10.2118/10103-PA

Krueger, R. F. (1988). SPE 17459 An Overview of Formation Damage and Well Productivity in Oilfield Operations: An Update. Society of Petroleum Engineers, (February), 535–553. https://doi.org/10.2118/10029-PA

Liot, O., Singh, A., Bacchin, P., Duru, P., Morris, J. F., & Joseph, P. (2018). Pore cross-talk in colloidal filtration. Scientific Reports, 8(1), 12460. https://doi.org/10.1038/s41598-018-30389-7

Liu, Q., Sun, Z., & Santamarina, J. C. (2019). Transport and Adsorption of Silica Nanoparticles in Carbonate Reservoirs: A Sand Column Study. Energy and Fuels, 33(5), 4009–4016. https://doi.org/10.1021/acs.energyfuels.9b00057

Marin, A., Lhuissier, H., Rossi, M., & Kähler, C. J. (2018). Clogging in constricted suspension flows. Physical Review E, 97(2), 21102. https://doi.org/10.1103/PhysRevE.97.021102

Mazutis, L., Gilbert, J., Ung, W. L., Weitz, D. A., Griffiths, A. D., & Heyman, J. A. (2013). Single-cell analysis and sorting using droplet-based microfluidics. Nature Protocols, 8(5), 870. https://doi.org/10.1038/nprot.2013.046

Mcdowell-boyer, L. M., Hunt, J. R., Itar, N., McDowell‐Boyer, L. M., Hunt, J. R., & Sitar, N. (1986). Particle transport through porous media. Water Resources Research, 22(13), 1901–1921. https://doi.org/10.1029/WR022i013p01901

Muecke, T. W. (1979). Formation Fines and Factors Controlling Their Movement in Porous Media. Journal of Petroleum Technology, 31(2), 1979. https://doi.org/10.2118/7007-PA

Mungan, N. (1965). Permeability Reduction Through Changes in pH and Salinity. Journal of Petroleum Technology, 17(12), 1965. https://doi.org/10.2118/1283-PA

Ryan, J. N., & Elimelech, M. (1996). Colloid mobilization and transport in groundwater. Colloids and Surfaces A: Physicochemical and Engineering Aspects, 107, 1–56. https://doi.org/10.1016/0927-7757(95)03384-X

Sakthivadivel, R., & Einstein, H. A. (1970). Clogging of porous column of spheres by sediment. Journal of the Hydraulics Division, 96(2), 461–472.

Sauret, A., Barney, E. C., Perro, A., Villermaux, E., Stone, H. A., & Dressaire, E. (2014). Clogging by sieving in microchannels: Application to the detection of contaminants in colloidal suspensions. Applied Physics Letters, 105(7), 074101. https://doi.org/10.1063/1.4893459

Sauret, A., Somszor, K., Villermaux, E., & Dressaire, E. (2018). Growth of clogs in parallel microchannels. Physical Review Fluids, 3(10), 104301. https://doi.org/10.1103/PhysRevFluids.3.104301

Sherard, J. L., Dunnigan, L. P., & Talbot, J. R. (1984). Basic properties of sand and gravel filters. Journal of Geotechnical Engineering, 110(6), 684–700.

Valdes, J. R., & Carlos Santamarina, J. (2007). Particle transport in a nonuniform flow field: Retardation and clogging. Applied Physics Letters, 90(24). https://doi.org/10.1063/1.2748850

Valdes, J. R., & Santamarina, J. C. (2006). Particle clogging in radial flow: microscale mechanisms. SPE Journal, 11(02), 193–198. https://doi.org/10.2118/88819-PA

Valdes, J. R., & Santamarina, J. C. (2008). Clogging: bridge formation and vibration-based destabilization. Canadian Geotechnical Journal, 45(2), 177–184. https://doi.org/10.1139/T07-088

Valdya, R. N., & Fogler, H. S. (1992). Fines Migration and Formation Damage: Influence of pH and Ion Exchange. SPE Production Engineering, 7(04), 325–330. https://doi.org/10.2118/19413-pa

Van Zwieten, R., Van De Laar, T., Sprakel, J., & Schroën, K. (2018). From cooperative to uncorrelated clogging in cross-flow microfluidic membranes. Scientific Reports, 8(1), 5687. https://doi.org/10.1038/s41598-018-24088-6

Wyss, H. M., Blair, D. L., Morris, J. F., Stone, H. A., & Weitz, D. A. (2006). Mechanism for

clogging of microchannels. Physical Review E, 74(6). https://doi.org/10.1103/PhysRevE.74.061402

You, Z., Bedrikovetsky, P., Badalyan, A., & Hand, M. (2015). Particle mobilization in porous media: Temperature effects on competing electrostatic and drag forces. Geophysical Research Letters, 42(8), 2852–2860. https://doi.org/10.1002/2015GL063986